



This is a repository copy of *Mechanosynthesis of disordered rock salt structures: thermodynamic and kinetic considerations*.

White Rose Research Online URL for this paper:

<https://eprints.whiterose.ac.uk/203504/>

Version: Published Version

Article:

Zhi, X. orcid.org/0000-0003-4416-7737 and West, A.R. orcid.org/0000-0002-5492-2102
(2023) *Mechanosynthesis of disordered rock salt structures: thermodynamic and kinetic considerations*. *Chemistry of Materials*, 35 (17). pp. 6790-6798. ISSN 0897-4756

<https://doi.org/10.1021/acs.chemmater.3c01080>

Reuse

This article is distributed under the terms of the Creative Commons Attribution (CC BY) licence. This licence allows you to distribute, remix, tweak, and build upon the work, even commercially, as long as you credit the authors for the original work. More information and the full terms of the licence here:

<https://creativecommons.org/licenses/>

Takedown

If you consider content in White Rose Research Online to be in breach of UK law, please notify us by emailing eprints@whiterose.ac.uk including the URL of the record and the reason for the withdrawal request.



eprints@whiterose.ac.uk
<https://eprints.whiterose.ac.uk/>

Mechanosynthesis of Disordered Rock Salt Structures: Thermodynamic and Kinetic Considerations

Xuan Zhi and Anthony R. West*



Cite This: *Chem. Mater.* 2023, 35, 6790–6798



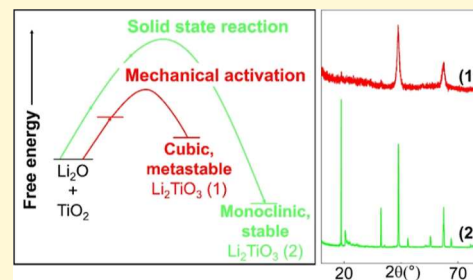
Read Online

ACCESS |

Metrics & More

Article Recommendations

ABSTRACT: Oxide phases with a cation-disordered, cubic rock salt structure that can be prepared by mechanochemistry include Li_2TiO_3 , Li_2MnO_3 , Li_3NbO_4 , and a new polymorph of LiAlO_2 . They are all metastable and transform irreversibly to thermodynamically stable ordered structures on heating. Li_2TiO_3 , Li_2MnO_3 , and Li_3NbO_4 form cubic solid solutions by doping with LiF; depending on the composition, they may be stable or metastable thermodynamically. Factors that control the thermodynamic and kinetic stability of phases and their synthesis conditions are reviewed.



INTRODUCTION

Thermodynamic and Kinetic Considerations. The methods used to synthesize materials, especially new materials, require an understanding of both thermodynamic and kinetic factors. High-temperature solid-state reaction usually leads to products that are thermodynamically stable, although reaction rates may be slow, depending on conditions, especially temperature. Low-temperature syntheses are important for several reasons, including a reduction in energy costs and also because a wide range of thermodynamically metastable materials and structures may be produced that cannot be prepared, or would decompose, at higher temperatures.

The methods that are used to synthesize solid-state materials and their subsequent stabilities are governed by a combination of thermodynamic and kinetic factors. Thermodynamically stable materials are those that have the lowest free energy for a given set of conditions, particularly temperature and pressure. All other materials that have the same composition but different structures are metastable under the same conditions. Kinetically stable materials are those that do not readily transform into a more stable structure because they have insufficient energy to overcome a particular activation energy barrier. This activation barrier confers metastability on the kinetically stable compositions or structures.

Equilibrium phase diagrams (if they are known) give no information on kinetics of formation or reaction rates but summarize the range of conditions, especially temperature, over which particular phases are thermodynamically stable or whether they should, in principle, decompose to give product(s) of lower free energy. They give information on phase stoichiometries and whether they are fixed or variable over certain composition or temperature ranges; they also show melting behavior, whether congruent or incongruent, and

whether phases undergo temperature-dependent, reversible, polymorphic phase transitions.

All reactions, whether the products are stable or metastable, proceed in the direction of a reduction in overall free energy. This means that the free energy of a starting reaction mixture, ΔG_R , must be higher than that of reaction products, as shown schematically in Figure 1 for a metastable product ΔG_A or a stable product ΔG_B . The reaction pathway that is followed

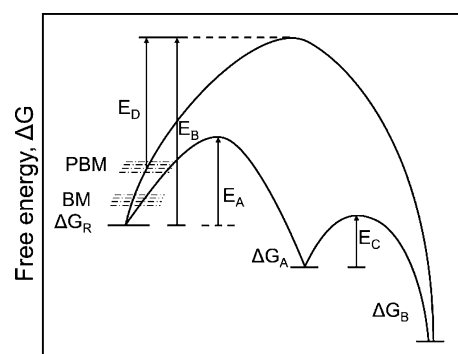


Figure 1. Schematic free energies of starting reagents, ΔG_R , and possible reaction products, ΔG_A and ΔG_B , with activation energies for reactions or transformations, E_A , E_B , and E_C . The reactant free energy can be raised by BM and PBM, giving a reduced activation energy, E_D .

Received: May 8, 2023

Revised: August 7, 2023

Published: August 25, 2023



preferentially is the one that has the lowest activation barrier, E_A , rather than the one, E_B , that gives a product with lower free energy, ΔG_B . Frequently, reactions occur in stages, often referred to as Ostwald's law of successive reactions,¹ in which intermediate, metastable phases form before the final, thermodynamically stable product. In Figure 1, product A is metastable and should transform subsequently to B, but in order to do so the activation barrier E_C must be overcome which affects the rate and conditions for the transformation from A to B. The choice of starting materials and perceived reaction pathway are vital considerations, even though appropriate thermodynamic data on free energies of formation and kinetic data on activation energies are rarely available.

For a given set of reactants, the magnitude of the activation barrier to form the products, E_A or E_B , is greatly influenced by possible structural similarities between reactants and products. In cases where there is good 2D structural similarity between the product and one of the reactants, with matching lattice dimensions in certain orientations, epitactic reactions may occur in which oriented growth of the product occurs on the surface of the reactant. This is because structural similarities between the reactant and the product at this interface greatly reduce the activation energy to nucleate the product. In cases that have a 3D structural similarity, topotactic reactions may occur, such as ion-exchange reactions in layered clay mineral structures. The 3D structural framework is unchanged during ion exchange, and although the overall composition changes during the reaction, the activation energy is low because nucleation stages are avoided.

Activation energies can also be reduced by injecting energy into reactants to raise their free energies, $\Delta G_{R'}$ as shown schematically for ball-milled, BM, and planetary ball-milled, PBM reactants in Figure 1, leading to a reduced activation energy, E_D . A common feature of many solid-state syntheses is the BM of reactants to reduce their particle size, increase the overall particle surface area, bring more reactant particles into contact, and thereby increase rates of nucleation. Solid-state reactions are surface-controlled during nucleation; the subsequent growth stages involve counter-diffusion of ions across interfaces and through products. With reduced particle sizes, diffusion distances are reduced which has the effect of increasing reaction rates. Consequently, it is possible to identify several effects of BM and PBM on reaction rates: (i) increased surface area of reactants, (ii) reduced diffusion distances, and (iii) activation of reactants by absorption of mechanical energy. The absorption of mechanical energy is, however, difficult to characterize and quantify. It is different from the absorption of thermal energy associated with the increase in temperature, but it also leads to increases in defect structures, vibrational energy, disorder, and entropy.

A fourth related factor is that the free energy of surfaces is generally higher than that of bulk crystal interiors because ions are in irregular or incomplete coordination environments at surfaces and often are not fully stabilized. This leads to a balance between the free energies of surfaces and the bulk, or product interiors, and to the well-established concept of critical size of nuclei. For nuclei of critical size, their surface free energy equals that of their bulk free energy. A reduction in the overall free energy can be achieved either by growth of the nuclei, in which the total surface area and surface free energy decrease as the bulk free energy increases, or by dissolution of the nuclei and the loss of their positive free energy of formation to the surrounding medium of lower free energy. An

additional effect of ball-milling is therefore to raise the total surface area and free energy of reactants. Conventional BM can reduce particle sizes to micron-sized dimensions. High-energy PBM is able to reduce particle sizes even further, as well as giving reactants, transition states, and subsequent products, that may have amorphous or highly defective structures.

Although Figure 1 shows products A and B that have lower free energy than reactants or reactant mixtures, it is possible to carry out the reverse process by providing an additional source of energy to obtain a metastable product from stable starting materials. Many examples are known of the de-intercalation of cathode materials during charging of lithium-ion batteries. For instance, during charging of the thermodynamically stable LiCoO_2 cathode, Li^+ ions are de-intercalated and some Co^{3+} ions are ionized to give Co^{4+} in $\text{Li}_{1-x}\text{CoO}_2$. The structural integrity of the layered rock salt structure is retained, and although the product is kinetically stable under battery operating conditions, it is only metastable thermodynamically. Effectively, the de-intercalation reaction is driven uphill to a state of higher free energy, Figure 2.

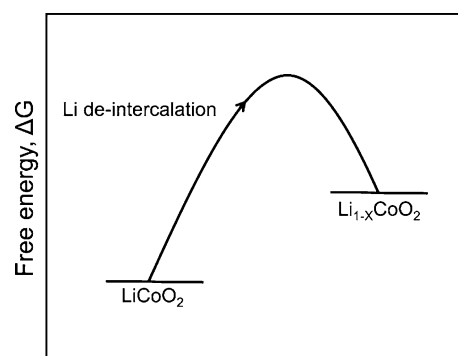


Figure 2. Schematic free energy change during charging the LiCoO_2 lithium-battery cathode.

The driving force for deintercalation comes from application of the charging voltage. Electrochemical redox reactions have an open-circuit voltage, OCV, which is related to the reaction free energy, ΔG° , by $\Delta G^\circ = -nFE^\circ$, where n is the number of electrons transferred, F is the Faraday constant, and E° is the cell OCV under standard conditions. To charge a battery, application of a voltage somewhat in excess of E° is required, and this gives a product with higher free energy, as shown schematically in Figure 2; the reaction is reversed during subsequent discharge.

A wide range of low temperatures or “chimie douce” routes for materials synthesis have been studied. Many involve, as a first step, the homogenization of reaction starting materials to give either a single-phase liquid solution or a precursor phase that has elements in the same ratio as in the desired products. This homogenization, which is typically what happens in sol-gel reactions, brings all reactants into contact at the atomic scale and avoids the long-range diffusion processes that are the main rate-limiting factor associated with the solid-state reaction of powder mixtures. While a liquid solution is usually thermodynamically stable, this certainly may not be the case once the solvent has been removed to leave (hypothetically) a residue that is often disordered, poorly crystalline, or amorphous. Such a residue has high free energy, similar in principle to the early stages of PBM, Figure 1, and is able to react rapidly, with a reduced activation energy. The reaction

often involves crystallization of a product that often has the same composition and, by avoiding the necessity for long-range diffusion, this reduces the activation energy for reaction. The enthalpy of formation of the crystalline product is, of course, the main driving force, since energy is released by the gain in lattice energy on crystallization of the product, but frequently metastable phases are produced by these low-temperature and low-activation energy *chimie douce* methods.

In addition to enthalpy changes, a second factor that influences reaction pathways and kinetics is the entropy of reactants, reaction intermediates, and products. The presence of disorder in a crystalline product may increase its free energy of formation, ΔG_f , through increased (positive) configurational entropy, S , in the equation $\Delta G_f = \Delta H_f - T\Delta S$. High-entropy materials, such as cation-disordered rock salt structures, are stabilized, often thermodynamically, by their high positive entropy which contributes, via the term $-T\Delta S$, to a negative ΔG_f . If both a negative ΔH and a positive ΔS contribute to a reduction in ΔG , formation of the product is clearly favorable thermodynamically. In other cases, ΔH associated with the introduction of structural disorder may be positive, but ΔG is lowered if the entropy term more than offsets the positive enthalpy term. It is important to try and distinguish, at least qualitatively, products that are thermodynamically stable from those that are “entropy-stabilized” but only metastable.

Entropy may also act to reduce activation energies of formation since intermediates or transition states in a reaction pathway may possess various amounts of disorder which act to reduce their free energy. This indicates why, under appropriate conditions and for two reasons, it is often possible to synthesize materials by low-temperature methods that are metastable and cannot be prepared by high-temperature processes: first, the free energy of the activated starting materials is raised and second the free energy of the transition state is reduced. A schematic example shown in Figure 3

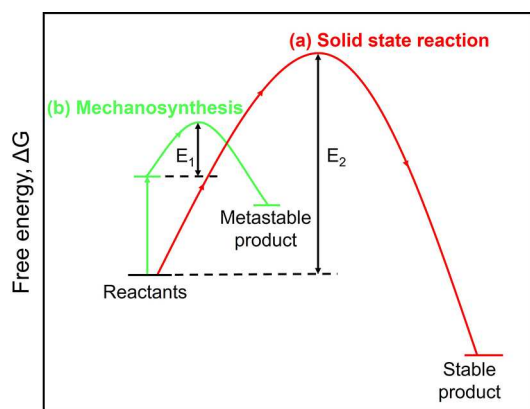


Figure 3. Schematic free energy reaction profile for two sets of reactions using the same reactants: (a) high-temperature solid-state reaction and (b) MS using PBM.

compares the free-energy changes involved in the (a) solid-state reaction of starting materials in their “ground state” to form a thermodynamically stable product and (b) mechano-synthesis (MS) or *chimie douce* of “activated” starting materials, to give a product that may be thermodynamically metastable relative to both the ground state starting materials and an alternative, thermodynamically stable product. The activation energy E_1 is much less than E_2 .

Mechanochemical synthesis or MS using PBM is a method that avoids the use of high temperatures. It is widely used in molecular chemistry for difficult organic syntheses, understanding shear processes in polymer lubricants, self-healing plastics,^{2–4} and main group chemistry syntheses.⁵ For solid-state reactions, MS is a relatively new method for oxide synthesis which avoids the traditional use of high temperatures and also enables the synthesis of new materials that may not be thermodynamically stable.^{6–13} It is a deceptively simple process in which mixtures of powder reactants are subjected to high-energy BM for extensive periods of time. The temperature usually rises by only a few degrees above room temperature but atomic-scale homogenization can occur to give single-phase products. Product particle sizes are usually in the nanometer range, giving broad XRD powder patterns, but from which only limited structural information may be obtained. Possible contamination of the samples by the milling media that are used is a potential concern and needs to be balanced against the milling conditions and mechanical energies involved.

A variety of inorganic oxides and processes have been prepared by MS, including BaTiO₃,⁶ lead magnesium niobate and zirconate, PMN,^{7,8} highly porous materials,⁹ LaMnO₃ catalyst,¹⁰ ammonia synthesis,¹¹ metal hydrides,¹² and complex oxides.¹³ Organic halide perovskite solar cell materials have been prepared by MS, and the kinetics of reaction between PbCl₂ and CH₃NH₃Cl analyzed using XRD data collected at different milling times.¹⁴ This allowed parametrization of the reaction as a function of input power supply, thereby linking milling conditions to reaction dynamics; the method has possible applications to other mechanically induced reactions.

Here, we report and discuss several examples of oxide-structured materials in the cubic rock salt family produced by MS. These are of considerable interest as possible lithium-battery cathodes, and in one case mechanical activation has been used as part of the preparation procedure.¹⁵ The phases are either stable or metastable thermodynamically, and some are entirely new. We consider the criteria for distinguishing between thermodynamically stable and metastable products, given that, in most cases, relevant thermodynamic data and knowledge of the phase diagrams are incomplete or unavailable.

EXPERIMENTAL SECTION

MS used various reactant combinations which are listed in Table 1. Li₂O and Li₂O₂ were used as-received, but before use they were stored in desiccators to reduce possible atmospheric attack. Other reagents were dried at certain temperatures, then cooled to room

Table 1. Reagent, Purity, Supplier, and Drying Temperature

reagent	purity (%)	supplier	drying temperature (°C)
Li ₂ O ₂	90	Alfa Aesar	80 (in vacuum)
Li ₂ O	95	Aldrich	80 (in vacuum)
MnO	99	Aldrich	180
Mn ₂ O ₃	99	Aldrich	600–650
Mn ₃ O ₄	97	Aldrich	600
MnO ₂	99	Aldrich	180
Nb ₂ O ₅	99	Aldrich	180
TiO	99.9	Aldrich	
Ti ₂ O ₃	99.9	Alfa	
TiO ₂	99.9	Aldrich	900
Al ₂ O ₃	99	Aldrich	900

temperature, and stored in desiccators. Reaction mixtures in the range of 1–2 g were loaded into hardened, stainless-steel jars and milled with hardened, stainless-steel balls in a Fritsch P6 planetary ball mill with a rotation speed of 350 rpm for 20 h. A detailed study of the synthesis of Li_2MnO_3 by PBM and optimization of various experimental factors involved will be published elsewhere.

Products were analyzed by powder X-ray powder diffraction, XRD, using a Bruker D2 Phaser, with $\text{Cu K}\alpha$ radiation ($\lambda = 1.5418 \text{ \AA}$) for routine phase analysis, and particle size measurement from XRD line broadening compared with a Si standard and a STOE-STADI PSD with $\text{Mo K}\alpha_1$ radiation ($\lambda = 0.7093 \text{ \AA}$) for accurate lattice parameter determination.

RESULTS AND DISCUSSION

Li_2TiO_3 . Li_2TiO_3 is dimorphic. It has a monoclinic, layered rock salt structure at low temperatures¹⁶ that transforms reversibly to a cubic, cation-disordered rock salt structure above about 1210 °C.¹⁷ Using standard solid-state synthesis with reaction at 800 °C, the monoclinic phase was produced, Figure 4b. However, the cubic polymorph was prepared at

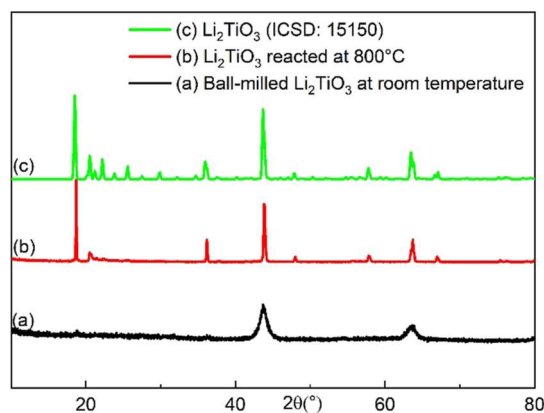


Figure 4. XRD patterns of Li_2TiO_3 prepared by (a) MS and (b) solid-state reaction at 800 °C, compared with (c) ordered Li_2TiO_3 (ICSD: 15150).

room temperature by MS, Figure 4a. It was kinetically stable but thermodynamically metastable and transformed gradually to the thermodynamically stable, ordered structure on heating above about 600 °C (not shown). On further heating, it would revert to the cubic structure above 1210 °C.

In the absence of accurate thermodynamic data on the free energy of the two polymorphs and their temperature dependence, it is not possible to say with certainty that the cubic polymorph at room temperature is metastable although it is clearly stable kinetically. However, since the order–disorder transformation occurs reversibly around 1210 °C, it is highly unlikely that a second, similar transformation also occurs at lower temperatures. There are examples in the literature where phases such as cubic, disordered Li_2TiO_3 prepared by chimie douce methods are referred to as low-temperature polymorphs. Strictly, they should be described as high-temperature polymorphs that can also be prepared at lower temperatures where they are kinetically stable but thermodynamically metastable. A characteristic of such metastable phases is that they should transform exothermically to the stable ordered polymorph on heating, but the transformation would not be reversible on subsequent cooling.

A useful way to represent qualitatively the relative stability of phases and their polymorphs is a schematic free energy–

temperature profile, shown for Li_2TiO_3 in Figure 5. At any temperature, the thermodynamically stable polymorph is

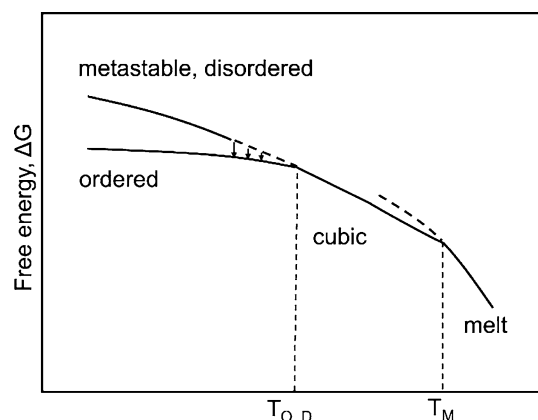


Figure 5. Schematic free energy–temperature profile for Li_2TiO_3 . The cubic polymorph is thermodynamically stable above 1210 °C but metastable at lower temperatures where it should transform to the thermodynamically stable, monoclinic, ordered rock salt structure. The rate of this transformation, shown as arrows, is kinetically controlled and depends on temperature.

represented by the solid lower curve and, therefore, Li_2TiO_3 transforms from ordered monoclinic to disordered cubic at the order–disorder transition temperature, T_{OD} , 1210 °C. At still higher temperatures, possibly 1600 °C, the cubic polymorph melts.

The slope of each curve is related to the entropy of that state. From $G = H - TS$, $\delta G/\delta T = -S$. Since

$$S_{\text{liq}} > S_{\text{disordered structure}} > S_{\text{ordered structure}}$$

the slopes of the three curves, Figure 5, become increasingly negative with increasing temperature, and especially the slopes change at the crossovers between ordered, disordered, and liquid phases.

Below 1210 °C, the cubic phase is metastable but can be obtained at lower temperatures where it is kinetically stable. It is represented by a dashed extension of the higher-temperature, stable cubic state since, in the absence of the disorder–order transformation, there is no discontinuity in thermodynamic properties of the disordered structure below T_{OD} . The undercooled disordered structure has higher entropy and free energy than the ordered structure and readily transforms to the ordered structure above about 600 °C, shown by arrows in Figure 5. At lower temperatures, the disordered structure is kinetically stable and does not readily transform to the ordered structure. Crystallization of molten Li_2TiO_3 would occur on rapid cooling of the melt below T_{M} , as shown by a short dashed extension of the liquid free energy curve below T_{M} , but it is unlikely that such melts could undercool significantly, become more viscous, and subsequently undergo a glass transition.

Li_2MnO_3 . Li_2MnO_3 has a monoclinic layered rock salt structure¹⁸ similar to Li_2TiO_3 , but there is no reported evidence that it can transform to a cubic polymorph at high temperatures. It is, however, possible to prepare nanoparticles with the cubic polymorph at room temperature by MS, Figure 6a(i), which transform gradually to the monoclinic polymorph on heating, (a)(ii)–(a)(v). During this process, the crystallite size increased greatly above 400 °C (Figure 6a,b), as shown by

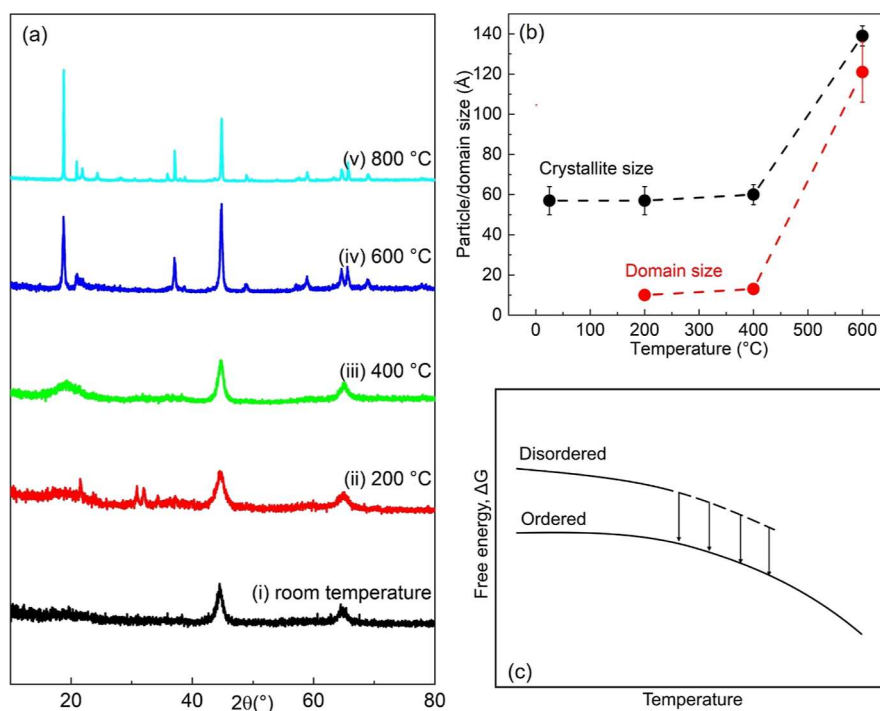


Figure 6. XRD patterns of Li_2MnO_3 : (a)(i) prepared by MS and [a(ii)–a(v)], after subsequent heating at various temperatures. (b) Crystallite and domain size after heating at different temperatures. (c) Schematic free energy–temperature profile.

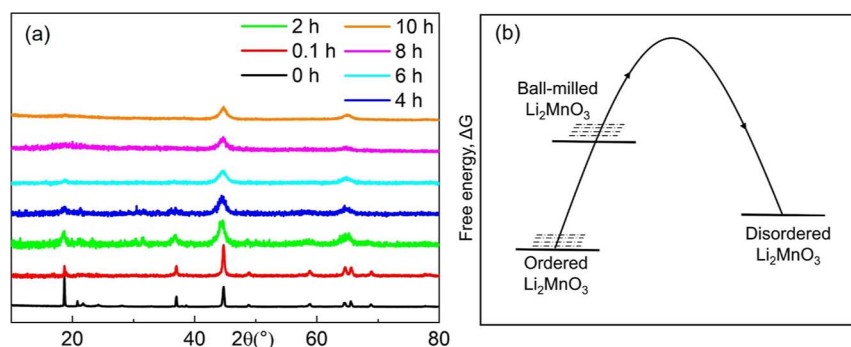


Figure 7. (a) XRD patterns showing the effect of high-energy BM on ordered Li_2MnO_3 and (b) schematic free energies of ordered, high-energy ball-milled and disordered Li_2MnO_3 .

a reduction in X-ray peak broadening. In addition, superstructure peaks that represented cation ordering started to emerge above about 200 °C. These were initially very broad, indicating a small ordered domain size, but became sharper at higher temperatures.

To describe the structure fully, it is therefore necessary to consider two size parameters, the size of the individual grains, each of which has a coherent, cubic close-packed oxide ion sub-lattice and the size of the cation-ordered domains which, initially, are much smaller than the grains. Both size parameters increase with annealing temperature until, at 800 °C, a fully ordered structure is apparent with no residual XRD line broadening of either ordered domain or individual grain diffraction peaks, indicating that the size of both is greater than $\sim 0.1 \mu\text{m}$. The variations of crystallite size and domain size with heating are shown in Figure 6b.

We have not investigated further the nature of cation ordering in the early stages, but note that, at 400 °C, especially the superstructure lines are extremely broad, Figure 6a(iii). It is possible that cation ordering occurs in two stages, first to form

alternate layers of Li and (Li, Mn), followed by a second stage at which cation ordering within the Li, Mn mixed layers becomes complete. It is not clear from the literature whether the structure(s) of the ordered polymorph is fully resolved, given the proposed role of stacking faults in observed intensity variations of some of the superlattice peaks in both Li_2TiO_3 and Li_2MnO_3 .¹⁸

In the absence of any information on the possible existence of a stable cubic polymorph at high temperature, the free energy–temperature profile of Li_2MnO_3 shows the stable monoclinic polymorph and a separate free-energy curve for the metastable cubic polymorph, Figure 6c, which changes to the stable polymorph, arrowed, at higher temperatures. It is not known whether the ordered polymorph melts directly or undergoes an order–disorder transition before melting.

Although a disordering transformation of Li_2MnO_3 has not been accomplished by heating ordered Li_2MnO_3 , it was induced by PBM ordered Li_2MnO_3 . Results for different milling times are shown in Figure 7a. The transformation has two notable features. First, a reduction in the intensity of

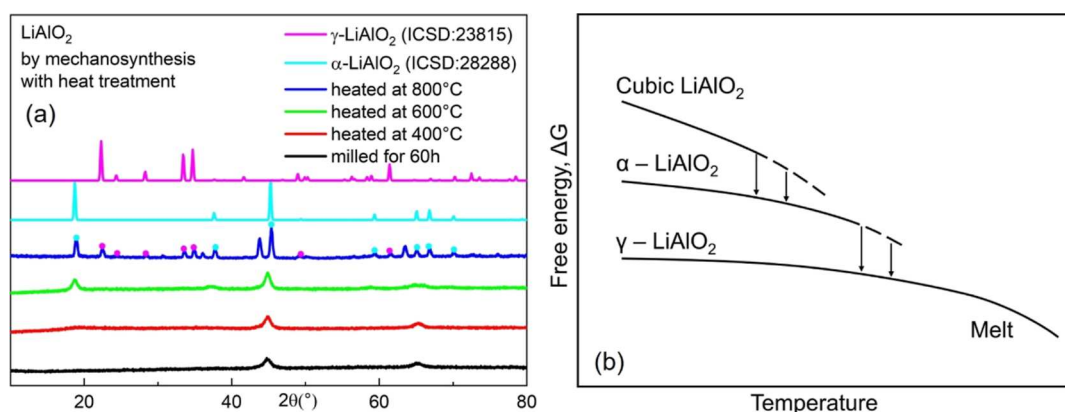


Figure 8. (a) XRD patterns of LiAlO_2 prepared by MS and subsequently heated at various temperatures and (b) schematic free energy–temperature profile for LiAlO_2 polymorphs.

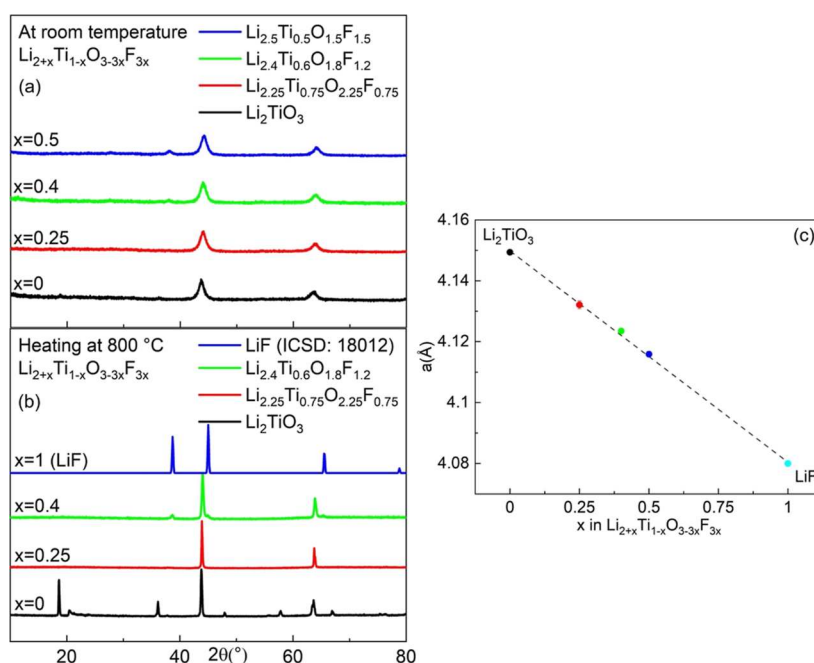


Figure 9. XRD patterns at room temperature of (a) cubic solid solutions between Li_2TiO_3 and LiF prepared by MS and (b) after subsequently heating the samples at 800 °C. (c) Linear variation of lattice parameter a against composition x at room temperature.

super-lattice lines is characteristic of the ordered structure. Second, a significant broadening of the sub-cell lines indicates a reduction in the crystallite size (Figure 7b). It appears that local cation disorder within the super-lattice domains either precedes or accompanies a reduction in crystallite and domain size, as judged by the XRD pattern after ~ 0.1 h of milling. The main super-lattice line at a 2θ of 19° has much reduced intensity but shows some broadening.

This order–disorder transition on ball-milling Li_2MnO_3 appears to be an example of an “uphill, stable–metastable transition” similar to that shown in Figure 2; the input mechanical energy from milling activates the free energy of ordered Li_2MnO_3 sufficiently to raise it above the free energy of the disordered structure, Figure 7b.

LiAlO_2 . Two polymorphs of LiAlO_2 are reported in the literature, a stable γ polymorph, which has a tetrahedral structure,¹⁹ and an α polymorph, which has an ordered layered rock salt structure similar to that of LiCoO_2 .²⁰ By MS, we prepared a new, third polymorph with a cubic disordered rock

salt structure, Figure 8. On subsequent heating at 400 °C, a very broad line indicative of ordered nano-domains can be seen. At 600 °C, the α structure is fully developed but still with small particle size. At 800 °C, a mixture of α and γ polymorphs is seen. We believe, but are not certain, that both cubic LiAlO_2 and α - LiAlO_2 are metastable polymorphs, as shown schematically in Figure 8b.

Oxyfluoride Solid Solutions: Li_2TiO_3 – LiF . The ionic radii of O^{2-} and F^- ions in octahedral coordination are very similar²¹ leading to the expectation that oxyfluoride rock salt solid solutions with disorder of both cation and anion sublattices may be possible, as has already been shown for $\text{Li}_2\text{MnO}_2\text{F}$ which is of considerable interest as a lithium-battery cathode.²² Using MS, the high-temperature cubic phase of Li_2TiO_3 forms an extensive solid solution with LiF and the general formula $\text{Li}_{2+x}\text{Ti}_{1-x}\text{O}_{3-3x}\text{F}_{3x}$ Figure 9a. The novelty here is that not only can the solid solution be prepared at ambient temperature by MS but some compositions are also stabilized thermodynamically, as shown in Figure 9b, by the

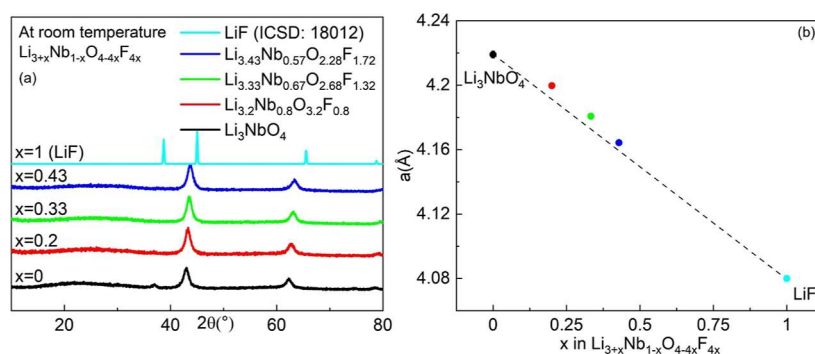


Figure 10. (a) XRD patterns of cubic solid solutions between Li_3NbO_4 and LiF . (b) Linear variation of lattice parameter a against composition x .

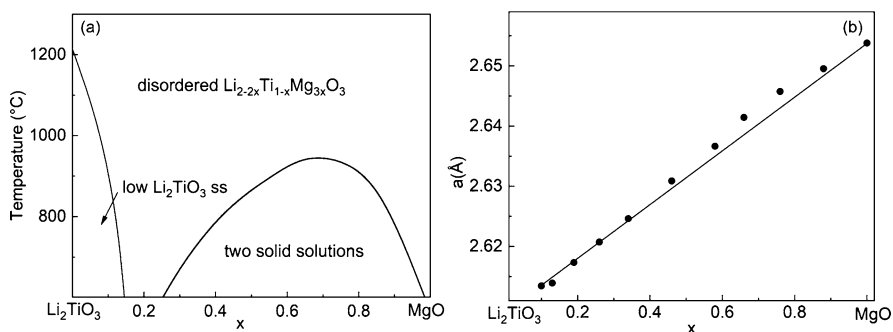


Figure 11. (a) Phase diagram of Li_2TiO_3 – MgO and (b) composition-dependence of unit cell parameter, a , adapted from ref 26.

effect of heating samples at 800 °C. Undoped Li_2TiO_3 , $x = 0$, becomes ordered after heating at 800 °C, whereas compositions $x = 0.25$ and 0.50 remain disordered. This means that the order–disorder transition temperature in Li_2TiO_3 has been reduced greatly from 1210 °C by solid solution formation with LiF . The range of disordered cubic solid solution formed by some compositions appears to be thermodynamically stable at ambient temperature and may also be regarded as entropy-stabilized.

Supporting evidence of doping and solid solution formation, with disorder on both cation and anion sublattices, is provided by the approximately linear variation of lattice parameter a with composition x , showing adherence to Vegard's law (Figure 9c). A small amount of LiF is shown in the XRD data for $x = 0.40$ (Figure 9b) and may be either a consequence of incomplete reaction during MS or because the doping limit exceeded under these conditions.

These results provide a clear example of entropy-driven formation of a thermodynamically stable solid solution range. The large gain in entropy associated with complete disorder on both anion and cation sites is more than sufficient to offset the enthalpy of formation of a partially ordered solid solution, irrespective of whether it is positive or negative. Data are shown for compositions $x = 0.25$, 0.40 , and 0.50 . It is, however, expected that a range of compositions close to Li_2TiO_3 , with $x < 0.25$, would show a partially ordered structure at lower temperatures, depending on the temperature–composition locus of the order–disorder transition, similar to that reported for the stabilization of cubic, disordered Li_2TiO_3 in solid solution with MgO ²³ (Figure 11). These results show the value of thermodynamic and phase diagram considerations in evaluating the thermodynamic/kinetic stabilities of doped materials that can potentially undergo order–disorder transformations.

Li_3NbO_4 and Oxyfluoride Solid Solutions. Li_3NbO_4 has an ordered rock salt structure containing clusters of Nb_4O_{16} edge-sharing octahedra.²⁴ Both Li_3NbO_4 and an extensive range of solid solutions with LiF were prepared by MS and shown by XRD to have a disordered cubic rock salt structure (Figure 10a). As far as we are aware, the metastable, disordered polymorph of Li_3NbO_4 has not been reported previously although cation-disordered solid solutions containing Mn, Fe, Co, and Ni as dopants have been reported.²⁵

The lattice parameter, a , of the solid solutions, $\text{Li}_{3+x}\text{Nb}_{1-x}\text{O}_{4-4x}\text{F}_{4x}$ showed a systematic decrease with x (Figure 10b). There is clear indication that the intermediate compositions have a slightly larger lattice parameter than expected from a line connecting values for Li_3NbO_4 and LiF . This positive deviation from Vegard's law implies a net repulsion within the disordered cation and anion arrangements, indicating a tendency to unmixing or immiscibility within the solid solutions and a preferential tendency for LiF -rich and Li_3NbO_4 -rich clusters to segregate.

Further studies on ball-milled samples with a complete range of x values that have been subsequently heated over a range of temperatures may show the existence of an immiscibility dome with an upper consolute temperature, as was found in the system Li_2TiO_3 – MgO ²⁶ (Figure 11). The Li_2TiO_3 – MgO phase diagram (Figure 11a) shows four consequences of the effect of entropy. First, the formation of an extensive range of solid solutions at high temperature, indicating that the large increase in entropy more than offsets any reduction in their enthalpy of formation. Second, stabilization of these solid solutions over a range of compositions to low temperatures, in preference to formation of a more extensive solid solution of ordered Li_2TiO_3 . Third, existence of an immiscibility dome over a range of compositions and temperatures. Inside the immiscibility dome, the entropy of a single phase solid solution is insufficient to overcome its enthalpy of formation, which

must be positive. Fourth, the significance of temperature in the $-T\Delta S$ term which illustrates entropy-controlled solid solution formation at high temperatures that reverts to enthalpy control at lower temperatures for a limited range of solid solutions. The phase diagram in Figure 11 may represent a common format for other materials that form both ordered and disordered rock salt structure phases and solid solutions.

CONCLUSIONS

Stoichiometric oxide phases such as Li_2TiO_3 , Li_2MnO_3 , Li_3NbO_4 , and LiAlO_2 can be prepared as cubic polymorphs with disordered rock salt structures by MS at room temperature where they are thermodynamically metastable but kinetically stable. PBM raises the free energy of the reactant mixtures, which effectively reduces the activation energy for reaction and facilitates the formation of a high configurational entropy, disordered phase as the first product of reaction.

The effect of mechanical energy on the free energy of phases is illustrated by the BM of cation-ordered, monoclinic Li_2MnO_3 . Mechanical energy input leads to disordering of the cation arrangement and a metastable cubic polymorph that has a disordered rock salt structure. The introduction of disorder into an ordered structure by mechanical activation is not new and is well known in alloy structures such as Ni_3Al . Introduction of disorder is the first step in amorphization of the alloy and is reversible by suitable heat treatment.²⁸ It is an uphill, stable-to-metastable process on comparing the relative free energies of ordered and disordered polymorphs, similar to the charging of lithium-ion batteries which involves application of a voltage that exceeds the decomposition potential, E° , of the cathode, Figure 2. LiCoO_2 itself is thermodynamically stable, but the de-intercalated product, $\text{Li}_{1-x}\text{CoO}_2$, is only metastable and readily re-intercalates to reform the stable structure and composition during subsequent battery discharge.

Cubic Li_2TiO_3 is metastable at room temperature and reverts to the stable, ordered polymorph on heating. At still higher temperatures, $>1210^\circ\text{C}$, the ordered polymorph undergoes an order–disorder phase transition, and the cubic polymorph becomes thermodynamically stable. The cubic polymorphs of the other three phases studied here are all thermodynamically metastable but kinetically stable at room temperature; as yet, there is no evidence whether they may, or may not, also form stable disordered polymorphs before melting.

The interplay between the enthalpy of formation of a phase or solid solution and any change in entropy is illustrated by the effects of doping Li_2TiO_3 with (i) LiF and (ii) MgO and the associated temperature–composition equilibrium phase diagrams. An increase in entropy favors the formation of disordered structures, especially at high temperatures. This also accounts for the appearance of low-temperature immiscibility domes in solid solution phase diagrams with an upper consolute temperature in which the entropy of mixing at lower temperatures is insufficient to offset a positive enthalpy of mixing; instead, unmixing of a solid solution into two phases occurs with decreasing temperature.

The thermodynamic principles that underlie phase diagrams and phase transitions, including order–disorder processes are well-established.²⁷ Here, we present practical guidelines and considerations into the use of thermodynamics, phase diagrams, and order–disorder transformations of solid solution

systems that can help to rationalize different materials synthesis methods, especially for stable or metastable materials that can be made by MS.

There is much current interest in oxyfluoride solid solutions with a disordered rock salt structure for possible lithium battery cathode applications. Their thermodynamic and kinetic stabilities may be assessed readily by the effect of heat treatment on materials made by MS.

A “hot topic” in the area of disordered structures concerns “high-entropy alloys (HEA)” exemplified by cation-disordered, rock-salt-structured solid solutions, MO, where M represents equimolar amounts of five similar-sized divalent cations, typically Mg, Co, Ni, Cu, and Zn. Originally, these were prepared by a high-temperature reaction^{29–31} but more recently have also been prepared by MS.³² They may be regarded as a compositional example of disordered rock salt materials typical of those discussed here in which (i) cation valences are not limited to divalent but range from 1+ to 5+, with the proviso that the cation/oxygen ratio is 1:1 and electroneutrality holds, (ii) there is no requirement that the different cations should be present in equimolar proportions, although it has been shown that this may lead to maximized entropy,²⁹ (iii) some compositions are thermodynamically stable only at high temperatures, others are stable at all temperatures, and yet others are metastable but only at low temperatures, (iv) as well as cation-disordered HEA materials, anion disorder occurs readily in oxyfluorides with cation ratios adjusted to compensate for the different charges of similar-sized O^{2-} and F^- ions. We anticipate that the family of materials with both cation and anion disorder could be extended further by the incorporation of similar-sized nitride anions, N^{3-} .

AUTHOR INFORMATION

Corresponding Author

Anthony R. West – Department of Materials Science & Engineering, University of Sheffield, Sheffield S1 3JD, U.K.; orcid.org/0000-0002-5492-2102; Email: a.r.west@sheffield.ac.uk

Author

Xuan Zhi – Department of Materials Science & Engineering, University of Sheffield, Sheffield S1 3JD, U.K.; orcid.org/0000-0003-4416-7737

Complete contact information is available at: <https://pubs.acs.org/10.1021/acs.chemmater.3c01080>

Notes

The authors declare no competing financial interest.

ACKNOWLEDGMENTS

This work was supported by the Faraday Institution grant number FIRGO17.

REFERENCES

- (1) van Santen, R. A. The Ostwald Step Rule. *J. Phys. Chem.* **1984**, *88*, 5768–5769.
- (2) Faraday Discussion 170, Mechanochemistry, from functional solids to single molecules, Montreal (2014); mechanochemistry: fundamentals, applications and future, Cambridge (2022).
- (3) Norman, N. Chemists use the force. *Chem. World* **2018**, 46–49.
- (4) Friscic, T.; Mottillo, C.; Titi, H. M. Mechanochemistry for synthesis. *Angew. Chem., Int. Ed.* **2020**, *59*, 1018–1029.

- (5) Tan, D.; Garcia, F. Main group mechanochemistry: from curiosity to established protocols. *Chem. Soc. Rev.* **2019**, *48*, 2274–2292.
- (6) Xue, J.; Wang, J.; Wan, D. Nanosized barium titanate powder by mechanical activation. *J. Am. Ceram. Soc.* **2000**, *83*, 232–234.
- (7) Kuscer, D.; Holc, J.; Kosec, M.; Meden, A. Mechanochemical synthesis of lead magnesium niobate ceramics. *J. Am. Ceram. Soc.* **2006**, *89*, 3081–3088.
- (8) Wang, J.; Xue, J.; Wan, D. M.; Gan, B. K. Mechanically activating nucleation and growth of complex perovskites. *J. Solid State Chem.* **2000**, *154*, 321–328.
- (9) Szczesniak, B.; Borysiuk, S.; Choma, J.; Jaroniec, M. Mechanochemical synthesis of highly porous materials. *Mater. Horiz.* **2020**, *7*, 1457–1473.
- (10) Blackmore, R. H.; Rivas, M. E.; Eralp Erden, T.; Dung Tran, T.; Marchbank, H. R.; Ozkaya, D.; Briceno de Gutierrez, M.; Wagland, A.; Collier, P.; Wells, P. P. Understanding the mechanochemical synthesis of the perovskite LaMnO_3 and its catalytic behaviour. *Dalton Trans.* **2020**, *49*, 232–240.
- (11) Han, G. F.; Li, F.; Chen, Z. W.; Coppex, C.; Kim, S. J.; Noh, H. J.; Fu, Z.; Lu, Y.; Singh, C. V.; Siahrostami, S.; et al. Mechanochemistry for ammonia synthesis under mild conditions. *Nat. Nanotechnol.* **2021**, *16*, 325–330.
- (12) Huot, J.; Cuevas, F.; Deledda, S.; Edalati, K.; Filinchuk, Y.; Grosdidier, T.; Hauback, B. C.; Heere, M.; Jensen, T. R.; Latroche, M.; et al. Mechanochemistry of metal hydrides: recent advances. *Materials* **2019**, *12*, 2778–2822.
- (13) Zyryanov, V. V. Mechanochemical synthesis of complex oxides. *Russ. Chem. Rev.* **2008**, *77*, 105–135.
- (14) Gil-Gonzalez, E.; Perez-Maqueda, L.; Sanchez-Jimenez, P. E.; Perejon, A. Paving the Way to Establish Protocols: Modeling and Predicting Mechanochemical Reactions. *J. Phys. Chem. Lett.* **2021**, *12*, 5540–5546.
- (15) Freire, M.; Lebedev, O. I.; Maignan, A.; Jordy, C.; Pralong, V. Nanostructured Li_2MnO_3 : a disordered rock salt type structure for high energy density Li ion batteries. *J. Mater. Chem. A* **2017**, *5*, 21898–21902.
- (16) Dorrian, J. F.; Newnham, R. E. Refinement of the structure of Li_2TiO_3 . *Mater. Res. Bull.* **1969**, *4*, 179–183.
- (17) Izquierdo, G.; West, A. R. Phase equilibria in the system $\text{Li}_2\text{O}-\text{TiO}_2$. *Mater. Res. Bull.* **1980**, *15*, 1655–1660.
- (18) Boulineau, A.; Croguennec, L.; Delmas, C.; Weill, F. Reinvestigation of Li_2MnO_3 Structure: Electron Diffraction and High Resolution TEM. *Chem. Mater.* **2009**, *21*, 4216–4222.
- (19) Marezio, M. The crystal structure and anomalous dispersion of $\gamma\text{-LiAlO}_2$. *Acta Crystallogr.* **1965**, *19*, 396–400.
- (20) Marezio, M.; Remeika, J. P. High-Pressure Synthesis and Crystal Structure of $\alpha\text{-LiAlO}_2$. *J. Chem. Phys.* **1966**, *44*, 3143.
- (21) Shannon, R. D. Revised effective ionic radii and systematic studies of interatomic distances in halides and chalcogenides. *Acta Crystallogr., Sect. A: Cryst. Phys., Diff., Theor. Gen. Crystallogr.* **1976**, *32*, 751–767.
- (22) House, R. A.; Jin, L.; Maitra, U.; Tsuruta, K.; Somerville, J. W.; Fürstermann, D. P.; Massel, F.; Duda, L.; Roberts, M. R.; Bruce, P. G. Lithium manganese oxyfluoride as a new cathode material exhibiting oxygen redox. *Energy Environ. Sci.* **2018**, *11*, 926–932.
- (23) Castellanos, M.; West, A. R. Order-disorder phenomena in oxides with rock salt structures: the system $\text{Li}_2\text{TiO}_3\text{-MgO}$. *J. Mater. Sci.* **1979**, *14*, 450–454.
- (24) Ukei, K.; Suzuki, H.; Shihido, T.; Fukuda, T. Li_3NbO_4 . *Acta Cryst. C* **1994**, *50*, 655–656.
- (25) Yabuuchi, N.; Takeuchi, M.; Nakayama, M.; Shiiba, H.; Ogawa, M.; Nakayama, K.; Ohta, T.; Endo, D.; Ozaki, T.; Inamasu, T.; Sato, K.; Komaba, S. High capacity electrode materials for rechargeable lithium batteries: Li_3NbO_4 -based system with cation-disordered rock salt structure. *Proc. Natl. Acad. Sci. U.S.A.* **2015**, *112*, 7650–7655.
- (26) Castellanos, M.; West, A. R. Deviations from Vegard's Law in Oxides Solid Solutions, The system $\text{Li}_2\text{TiO}_3\text{-MgO}$ and $\text{Li}_2\text{TiO}_3\text{-Na}_2\text{TiO}_3$. *J. Chem. Soc., Faraday Trans.* **1980**, *76*, 2159–2169.
- (27) Hillert, M. *Phase Equilibria, Phase Diagrams and Phase Transformations: Their Thermodynamic Basis*. Cambridge Press, 2nd ed. (2008)
- (28) Cahn, R. W. Disorder and reordering of mechanically milled superlattice alloys. *Bull. Mater. Sci.* **1999**, *22*, 175–180.
- (29) Rost, C. M.; Sachet, E.; Borman, T.; Moballeggh, A.; Dickey, E. C.; Hou, D.; Jones, J. L.; Curtarolo, S.; Maria, J.-P. Entropy-stabilized oxides. *Nat. Commun.* **2015**, *6*, 8485.
- (30) Sarkar, A.; Djenadic, R.; Usharani, N. J.; Sanghvi, K. P.; Chakravadhanula, V. S. K.; Gandhi, A. S.; Hahn, H.; Bhattacharya, S. S. Nanocrystalline multicomponent entropy stabilised transition metal oxides. *J. Eur. Ceram. Soc.* **2017**, *37*, 747–754.
- (31) Chen, H.; Fu, J.; Zhang, P.; Peng, H.; Abney, C. W.; Jie, K.; Liu, X.; Chi, M.; Dai, S. Entropy-stabilized metal oxide solid solutions as CO oxidation catalysts with high-temperature stability. *J. Mater. Chem. A* **2018**, *6*, 11129–11133.
- (32) Chen, H.; Lin, W.; Zhang, Z.; Jie, K.; Mullins, D. R.; Sang, X.; Yang, S.-Z.; Jafta, C. J.; Bridges, C. A.; Hu, X.; Unocic, R. R.; Fu, J.; Zhang, P.; Dai, S. Mechanochemical Synthesis of High Entropy Oxide Materials under Ambient Conditions: Dispersion of Catalysts via Entropy Maximization. *ACS Mater. Lett.* **2019**, *1*, 83–88.

Recommended by ACS

Solid-State Phase Transformation Explains the Mixed Crystallographic Character of $\text{Zr}(\text{Nb},\text{Fe})_2$ Nanoprecipitates in Zr-2.5Nb

Aditya Kamath, Laurent Karim Béland, et al.

AUGUST 31, 2023
THE JOURNAL OF PHYSICAL CHEMISTRY C

READ 

Hydrogarnet-Derived Porous Polyhedral Particles of $\text{SrFeO}_{3.8}$ Perovskite

Hikaru Otaguro, George Hasegawa, et al.

AUGUST 07, 2023
CHEMISTRY OF MATERIALS

READ 

Selective Interstitial Hydration Explains Anomalous Structural Distortions and Ionic Conductivity in $6\text{H-Ba}_4\text{Ta}_2\text{O}_9 \cdot 1/2\text{H}_2\text{O}$

Frederick P. Marlton, Chris D. Ling, et al.

MARCH 20, 2023
CHEMISTRY OF MATERIALS

READ 

The Formation of Stacking Faults in Barium Zirconate-Type Perovskites

Dylan Jennings, Wolfgang Rheinheimer, et al.

AUGUST 04, 2023
CHEMISTRY OF MATERIALS

READ 

Get More Suggestions >